

# Pilot scale production of novel calcium sulfoaluminate cement clinkers and development of thermal model

Sameer Khare<sup>a1</sup>, Marcus C. Bannerman<sup>a</sup>, Fredrik P. Glasser<sup>b</sup>, Theodore Hanein<sup>a</sup>, Mohammed S. Imbabi<sup>a</sup>

(a) School of Engineering, University of Aberdeen, AB24 3UE, UK

(b) Department of Chemistry (NCS), University of Aberdeen, AB24 3UE, UK

## Abstract

Pilot scale trials were successfully performed on the production of novel calcium sulfoaluminate (CSA) cement clinker in a direct natural gas heated rotary kiln at the IBU-tec facility in Germany. A raw meal throughput of ~25 kg/h was fed to the rotary kiln heated by co-combustion of natural gas and elemental sulfur, with the latter serving as both fuel substitute and reactant, to partially or wholly replace gypsum as the source of sulfur in CSA production. A well-mixed heat transfer kiln model was developed to predict the overall kiln heat flux and gas temperature profiles, to account for gaseous radiative properties. The predicted gas temperature inside the kiln varied from 1566 K in the flame zone to 1019 K at the feed zone, with peak temperature approaching 1724 K. The combined emissivity of the CO<sub>2</sub> and H<sub>2</sub>O gas mixture varied between 0.13 and 0.2 at these temperatures for partial pressure ratio PH<sub>2</sub>O/PCO<sub>2</sub> of 1.7. The trial kiln has a low thermal efficiency of 3% of the total supplied energy.

The simplistic model provided approximate performance predictions for the KDO kiln and also for different kiln sizes and can help to establish the effects of operating parameters on heat transfer trends.

## Keywords

CSA cement clinker, rotary kiln, thermal performance, modelling, sulfur combustion

## 1. Introduction

Commercial production of Calcium SulfoAluminate (CSA) cement started in China in the 1970's and is practised worldwide [1]; however, CSA production via solid-gas reactions between gaseous oxides of sulfur and oxygen with the solids in the raw feed is a relatively

---

<sup>1</sup> Department of Chemical Engineering, University of Bath, UK  
s.p.khare@bath.ac.uk

new process technology. Traditionally, gypsum or anhydrite (a naturally occurring mineral, a manufactured material or an industrial by-product) is used in the raw meal to address clinker sulfur demand; however, elemental sulfur, which can be sourced from the sour gas stripping operation in which it is produced as a by-product, can provide partial or complete replacement of calcium sulfate. Cement manufacturing is a very energy intensive process and the use of waste sulfur has potential environmental benefits as a permanent means of capturing and immobilising sulfur. The lower calcium content in CSA compared to Portland cement can additionally save an estimated 200 kg/tonne of CO<sub>2</sub> emitted per tonne of cement produced and lessen the need for CO<sub>2</sub> intensive Portland cement [1]. It has the potential to reduce the thermal energy requirements from conventional hydrocarbon fuels because of reduced pyro processing temperature and also by burning sulfur and capturing the gases produced within the cement clinker product. Recent papers by Galan et al [2] and Hanein et al [3] summarise the experimental production of CSA using elemental sulfur. The concept of combusting elemental sulfur (to replace traditional gypsum and as an additional energy source), and utilising the waste heat is a step towards developing low carbon, or novel, green CSA cements. The transfer of sulfur absorption from vapour to solid and associated equilibria and kinetics are not considered here but will be described in detail in a subsequent work. The scope of this work is limited to predicting thermophysical balances during the kiln operation. Cement kilns are complex systems that involve complex physics, multiple phases and simultaneous reactions with different time scales during clinker formation. In literature, theoretical modelling of the flow field and combustion in cement kilns has been reported using commercial computation fluid dynamics CFD code [4] including radiation heat transfer and with reaction equilibria [5, 6]. There exist non-homogeneous and complex heat transfer interactions within the bed and the freeboard region of the kiln. Most of the published theoretical computational models predict the three main zones: the flame, the inner walls and the materials representing the rotary kiln operation. These zones are solved in isolation. The gas and the inner wall temperatures which determine the heat flux to the material (the charge) were approximated with one-dimensional model without detailed flame calculations.

Mastorakos et al [4] has reported to solve these modules iteratively and simultaneously using approximation on the boundary conditions to solve for heat flux. This further determines kiln operating parameters including the gas temperature for better understanding of kiln operation. It was identified that heat transfer by radiation was the dominant mode between gas and kiln inner walls with 40% of the supplied energy was transferred towards clinker formation. The model predictions gave qualitative agreement to the experimental data which was considered reasonable. Due to this complexity of integrating modules, existing literature has mainly focused on simple one-dimensional steady state models for heat transfer within rotary kilns which are shown to work well [7-9]. Therefore, this work focuses on a more simplistic zonal approach to calculate the overall thermal profile and efficiency. The current model entirely neglects the chemical and phase changes as well as their contribution to the thermal profiles.

This paper summarises the pilot-scale trial findings and provides a theoretical heat transfer model of the pilot scale kiln used during the trials with experimental validation. The usefulness of this model to carry out parametric studies and for evaluating scale-up performance is demonstrated.

## 2. Experimental analysis

### 2.1 Rotary kiln description

The KDO pilot scale kiln at IBU-tec is a 0.3 m internal diameter, 7.2 m in length horizontal rotary kiln featuring a direct fired natural gas burner; it was the kiln used during the production trial of novel CSA cement clinkers. The kiln's steel shell is lined with a 5 cm thick refractory cement. The process schematic includes a cyclone preheater, dust filter, kiln and cooler; the clinker dust was collected separately to close the material balance. Figure 1 shows a schematic of the pilot scale kiln. The design of an appropriate raw meal, described in the next section, was introduced from the feed side of the kiln and the elemental sulfur was fed through the flame side of the kiln, using a gravimetric screw feeder. Gas analysers at the raw feed side and after the scrubber were installed to monitor SO<sub>x</sub> emissions. The

observation glass window was located on the outer wall at the flame side of the kiln and adjacent to the gas burner which was axially placed (Figure 3b). The burner is inserted 1 m inside of the kiln. Thermocouple of Type-S (Pt10%Rh-Pt) were installed at 6 locations from flame side starting at 0.89, 1.35, 2.4, 4.1, 5.7, 7.2 m represented as location 1.1, 1.2 up to 5 respectively on the kiln to measure internal temperatures. The thermocouple manufacturer's reported permitted deviation was  $\pm 1.5$  C between 273 and 1873 K [10]. A detailed description is reported in [3].

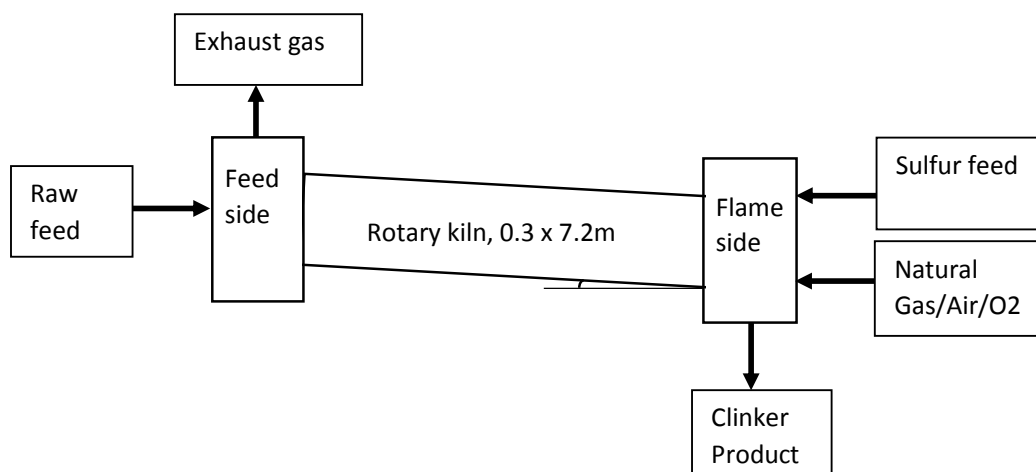


Figure 1. Schematic of pilot scale kiln, KDO.

## 2.2 Feed mix and product characterisation

The objective of designing the feed mix was to obtain CSA cement clinker with pre-defined product phases as reported in [3]. However, due to the limitations on feed stoichiometry arising from the composition of raw materials available in bulk, the closest achievable clinker product phase composition was 40% ye'elimite ( $C_4A_3S'$ ), 47% belite ( $C_2S$ ) and 10% ferrite ( $C_6A_2Fe$ ) by weight. The kiln was fed at a rate of 25 kg/hr with the raw-meal mix containing limestone, bauxite and clay. Table 1a shows the raw material analysis and Table 1b include the feed operating conditions. The oxides of sulfur were available in the gas phase in the kiln, by combusting elemental sulfur (99.9% pure) along with the natural gas feed.

The amount of sulfur used in the trial was determined by estimating the required partial pressures necessary to achieve sulfur absorption within the cement clinker and to stabilise

phases. The contribution of heat associated with sulfur combustion to the total heat requirement was minimal due to the low requirement of feed sulfur as well as a high excess natural gas feed rate used to maintain clinkering temperatures within the low efficiency (3%) kiln design with no option of heat recovery, but of course kiln efficiency is not the issue here. A detailed thermodynamic model for CSA cement clinker phases developed at the University of Aberdeen [11] was used to predict the raw meal composition for the production of CSA cement clinker and/or to test sulfur absorption through the gaseous phase by burning elemental sulfur. The oxide composition of the produced CSA clinker is reported in Table 2 and is close to the initial raw meal feed.

Table 1a. Raw material analysis, wt% (XRF analysis)

<b>Compound</b>	<b>Limestone</b>	<b>Clay</b>	<b>Bauxite</b>
CaO	55.7	0.87	0.16
Al <sub>2</sub> O <sub>3</sub>	-	38.2	69.32
SiO <sub>2</sub>	0.1	39.25	11.5
Fe <sub>2</sub> O <sub>3</sub>	0.009	6	1.2
MgO	0.26	-	-
SO <sub>3</sub>	-	-	-
K <sub>2</sub> O	-	0.6	0.45
TiO <sub>2</sub>	-	1.8	3.5

Table 1b. Operating conditions of the kiln

Raw meal feed (dry)	25 kg/hr
Feed temp/press	298 K / 1 atm
Natural gas feed	21.5 ± 0.3 m <sup>3</sup> /hr
Primary air	177 ± 7 m <sup>3</sup> /hr
Oxygen feed	3.8 ± 0.2 m <sup>3</sup> /hr
Sulfur feed	2.4 kg/hr

Table 2. Produced CSA clinker, wt% (XRF analysis) [3]

<b>Compound</b>	<b>Raw meal</b>	<b>CSA Product Clinker</b>
CaO	54.3	55.1
Al <sub>2</sub> O <sub>3</sub>	24.6	24.1
SiO <sub>2</sub>	17.4	17.4
Fe <sub>2</sub> O <sub>3</sub>	2.6	2.3
TiO <sub>2</sub>	1.2	1.1

### 2.3 Temperature measurements

During the trial the external wall surface temperatures of the kiln were measured. A handheld infrared thermal imaging IR camera (FLIR T660) was used to record kiln external

temperatures at regular intervals during operation as well as point measurement of internal temperature near the flame zone. The camera is capable of recording temperatures upto 2273 K and with an accuracy of  $\pm 1\%$  [12]. External surface measurements using IR camera were taken and validated with external thermocouple measurements. The locations of measurement points using the IR camera on the external wall surface were chosen in a way that ensured coincidence with the existing thermocouples points used to record the kiln's internal surface temperatures. Figure 2 shows the external thermal imaging of the KDO kiln in operation.

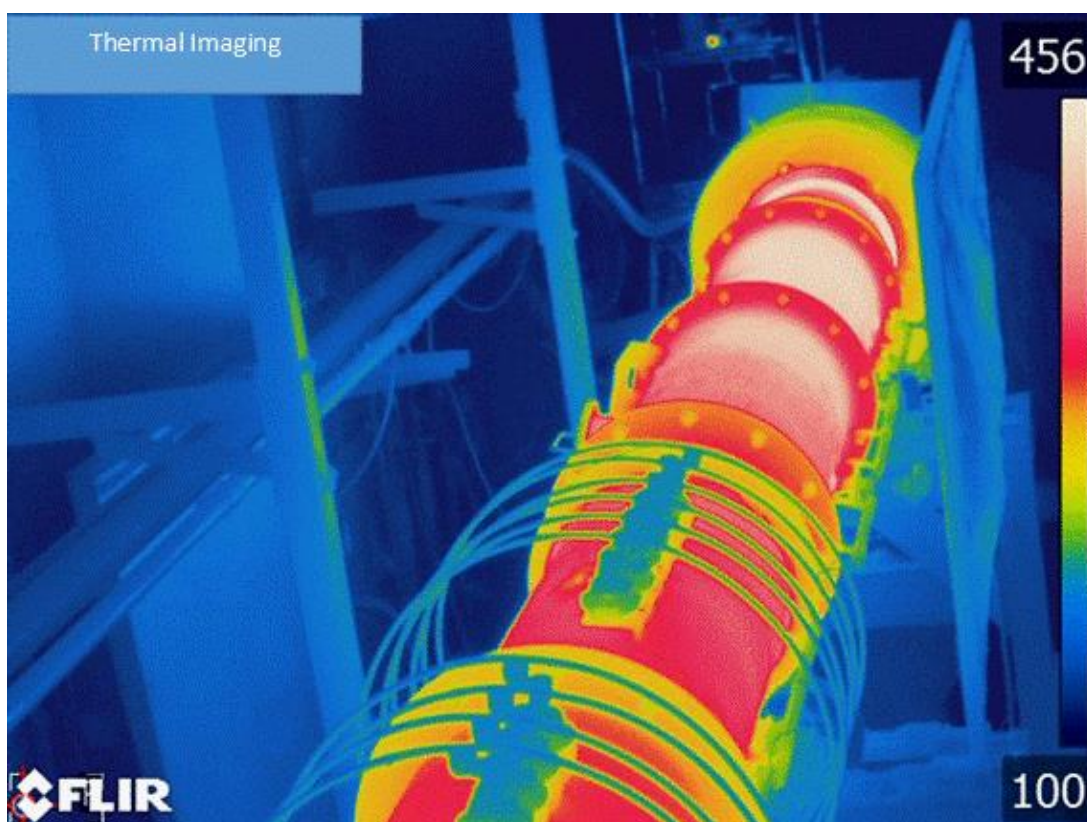


Figure 2. The external kiln surface thermal imaging along the length of the kiln during steady state production. Lower surface temperatures are at the lower bottom (feed side) with high temperature towards the top far end (flame side).

Figure 3 (a) shows thermal imaging and temperature measurement of the flame zone through the window near the flame zone looking inside the kiln during operation. Different locations inside the kiln were represented by point temperature measurements as shown.

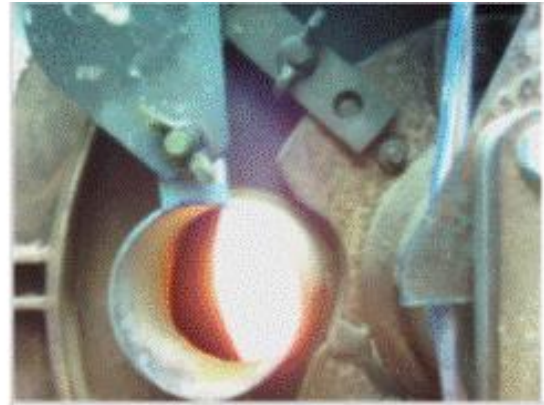
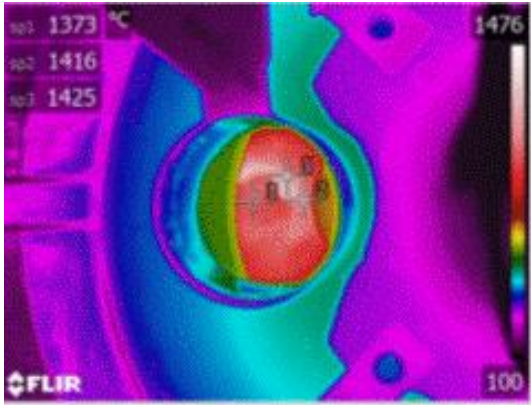


Figure 3. (a) Thermal imaging of the flame zone (b) Normal photograph of the flame zone. Two separate recordings each were made with IR camera and with external thermocouple measurement on the kiln external surface. The temperature for a single point or for a known area can be measured by specifying a number of parameters mainly the medium, surface emissivity, measurement distance, surrounding temperature, reflected temperature and relative humidity of the medium. The emissivity values of 0.85 supplied by the provider of pilot facility were used for the inner wall with similar values (0.9) reported in [4, 15] for the inner wall and bed material. The IR temperature of 1700 K around the flame zone is measured (Figure 3a). The values obtained are approximate as the camera receives radiation from the object as well from surroundings and the atmosphere within the line of sight. The measurement of objects at low temperature are more critical than measuring objects at high temperatures, since other radiation sources (such as surroundings and atmosphere present in between line of sight) are not significant in the latter case. Therefore, the error introduced during measuring high temperature flame object at close distance will be minimal.

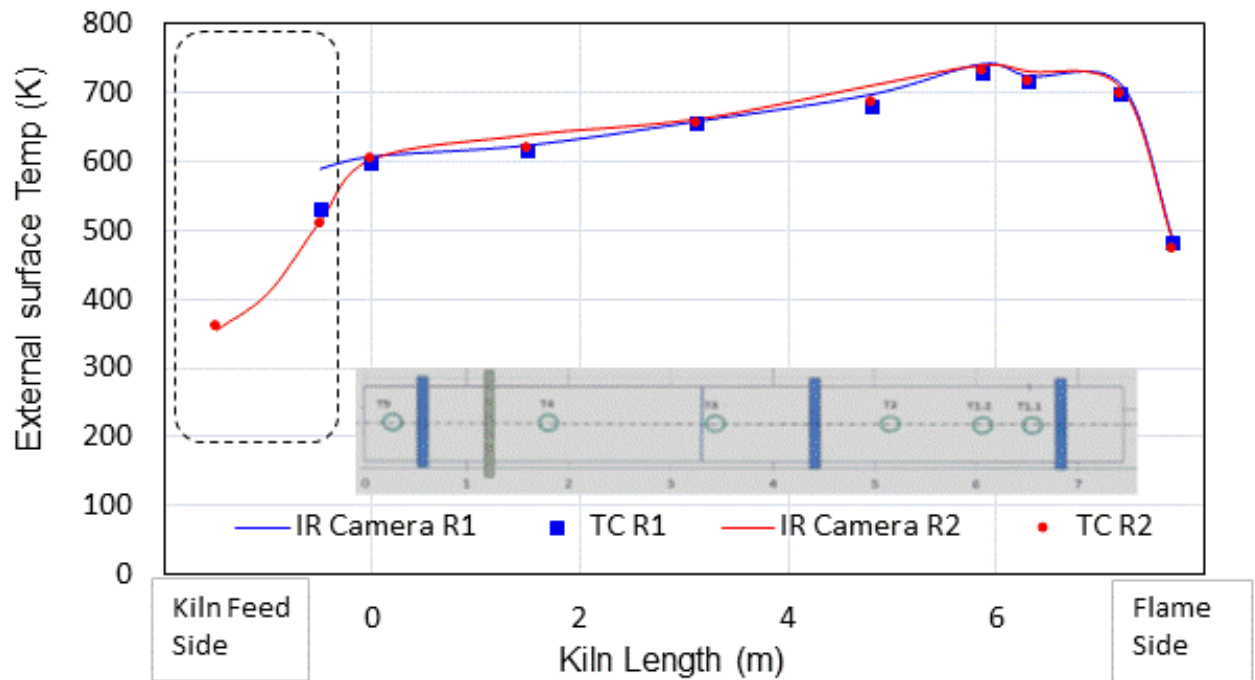


Figure 4. External surface temperature measurement of the pilot scale kiln during operation. The temperature measurement readings from both measurement tools were found to be in good agreement as shown in Figure 4. The peak temperature occurs near the flame region and slightly inwards of the flame end (product exit). The external surface temperature variation observed ranges from 720 K at the flame side to 600 K at the feed side. Extra temperature measurements were recorded towards the kiln feed side, down to 359 K, to represent the raw meal feed temperature conditions through a screw feeder via metal pipe just before entering the kiln section - see the marked rectangular area.

### 3. Theoretical analysis

#### 3.1 Radiative properties

Natural gas combustion within the cement kiln generates heat that is transferred from flame and combustion products to the surrounding furnace inner walls and the raw meal by radiation. Thermal radiation is thus the dominant mechanism for transferring heat from flame and combustion products. The combustion products usually consist of combustion gases, such as water vapour, carbon dioxide, sulfur oxides, nitrous oxides and particulates.

Estimation of the radiative properties of gaseous media (mainly  $\text{CO}_2$  and  $\text{H}_2\text{O}$ ) in the kiln involves estimating the partial pressures of these gaseous species. The natural gas was

fired with 10% excess air and pure oxygen volumetric flow of  $\sim 5\text{m}^3/\text{hr}$  was mixed with air to control the flame temperature. This resulted in partial pressures of water vapour and carbon dioxide of 0.17 and 0.1 respectively. Real gases absorb radiation in specific absorption bands of certain wavelengths (non-gray gases). In gray gases, absorption is independent of spectral location or wavelength. The relationship between real gas emissivity ( $\epsilon_{gas}$ ) and the gas partial pressure in the gas-path length product ( $P_p \cdot L$ ), also known as the optical path length, is the weighted sum-of-gray gas emissivity developed by Smith et al [13] is shown in Equation 4:

$$\epsilon = \sum_{i=0}^I a_{g,i} (T) [ 1 - e^{-k_i P_p L} ] \quad (1)$$

Where,

$a_{g,i}$  = Emissivity weighting factor for the  $i^{\text{th}}$  gray gas at Temperature

$k_i$  = absorption coefficient of  $i^{\text{th}}$  gray gas ( $\text{atm}\cdot\text{m}$ )<sup>-1</sup>

$[ 1 - e^{-k_i P_p L} ]$  =  $i^{\text{th}}$  gray gas emissivity with absorption coefficient  $k_i$

$P_p L$  = partial pressure-path length product ( $\text{atm}\cdot\text{m}$ )

$I$  = total number of gray gases

Smith et al [13] presented the polynomial coefficients and absorption coefficients for ratios of the partial pressure of water vapour to the carbon dioxide of 1 and 2. Table 3 gives the polynomial coefficients generated for  $\text{PH}_2\text{O}/\text{PCO}_2 = 2$ . These coefficients were generated for practical combustion systems with temperature ranging from 600 to 2400 K at a total pressure of 1atm with path length chosen range was 0.1 to 10 m.

Table 3. Polynomial coefficients for the 3-gray gas model for  $\text{H}_2\text{O}$  and  $\text{CO}_2$  mixture with  $\text{PH}_2\text{O}/\text{PCO}_2 = 2$ .

Gray gas, i	Absorption coefficient, $k_i$	$b_{e,j=1} \times 10^1$	$b_{e,j=2} \times 10^4$	$b_{e,j=3} \times 10^7$	$b_{e,j=4} \times 10^{11}$
1	0.4201	6.508	-5.551	3.029	-5.353
2	6.516	-0.2504	6.112	-3.882	6.528
3	131.9	2.718	-3.118	1.221	-1.612

The 3-gray-1-clear gas model (3-GGM) is used to estimate the emissivity of gases, which is then in turn used to estimate the kiln radiation heat transfer. The estimation of gas emissivity were corrected further according to Ketslakh et al [14]. This includes formulations for

determining the effective emissivity in heat exchange by radiation between the gases, material, and lining of the rotary kiln. The contribution of entrained solids on effective emissivity could be estimated using equation reported in [15]. However, Mujumdar et al [15] reported few experimental studies on solids entrainment suggesting the volume fraction of solids is very small (<1%) and for the smaller trial kiln currently used, the gas contribution towards total emissivity is dominant. Total gas emissivity was estimated for natural gas combustion in the course of rotary kiln operation. A theoretical gas emissivity estimation was made on the pilot scale rotary kiln KDO (K1) currently used for the CSA production as well as on three other hypothetical kilns (K2, K3 & K4) with varying sizes as shown in Table 4.

Table 4. Kiln sizes used in the study.

Kilns considered	Kiln Size (m)
K1 (KDO)	0.3 x 7.2
K2	0.6 x 4
K3	1 x 12
K4	2.7 x 60

Figure 5 shows the total gas emissivity predicted for the optical path length used as a function of temperature.

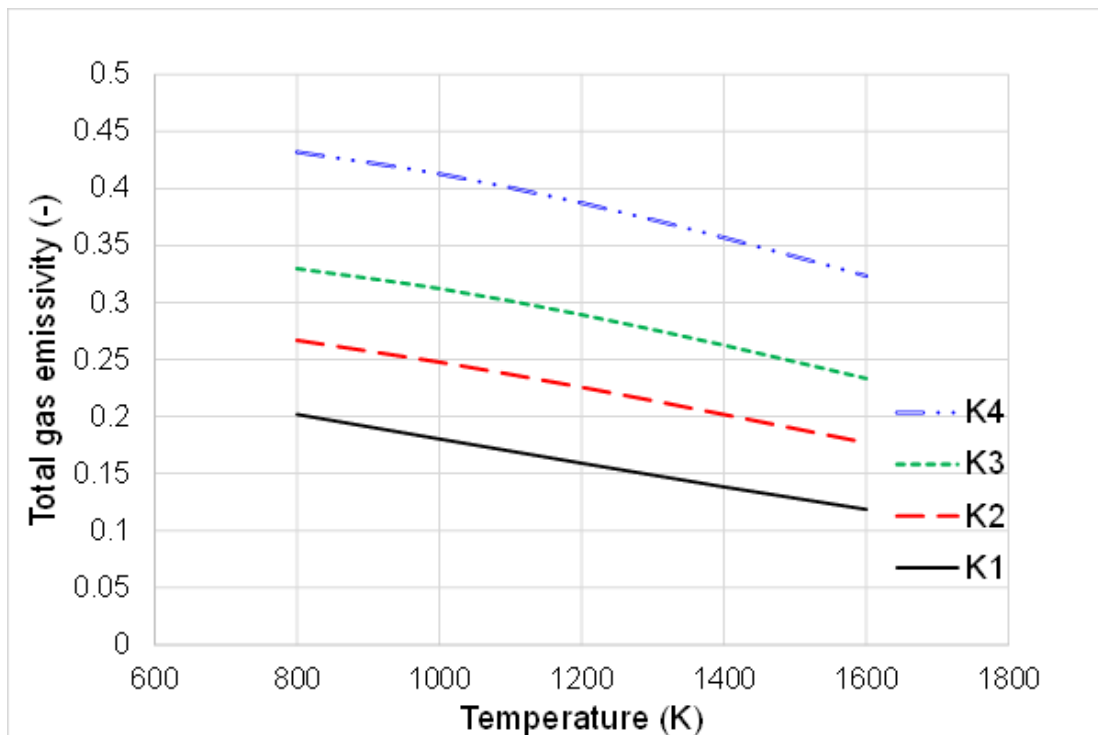


Figure 5. Gas emissivity profile as a function of temperature for various kiln sizes.

The emissivity of gas depends on the kiln size, the fuel type and combustion conditions used as well as the dust content of the medium. The contribution of gas emissivity increases for larger kilns. The effect of gas radiation from combustion products on the furnace heat transfer is evaluated using the well-stirred model, in which the combustion products filling the enclosure are treated as being isothermal and of constant composition.

### 3.2 Model description

The pilot scale rotary kiln KDO, is a cylindrical chamber with flue gases from natural gas combustion distributed across the cross-section. A well-mixed combustion model [16] is used to predict the overall heat transfer across the kiln for a given fuel feed rate and from a single gas temperature at the furnace exit or at an imaginary volume. The combustion products were assumed gray and at a single uniform temperature in a selected zone. The adiabatic flame temperature (AFT) with no heat loss to the surrounding was used as the starting temperature. The gas and inner wall radiative properties were assumed constant in that zone.

A complete heat transfer model can be built upon several cross-sectional heat transfer models to cover for the entire kiln [17]. These heat transfer sub-models depends primarily on the local temperature and also on all processes occurring within the kiln such as heat transfer between gas to exposed inner walls and bed material, exposed wall to wall and bed material, covered wall to covered bed material. Recently, CFD models are being applied to simulate rotary kilns [17, 18, 19]. However, the treatment of CFD models are limited to modelling the freeboard region with separate coupling to a one-dimensional model for the bed [18].

Typically, in the rotary kiln, the heating zone occupies the significant portion of the kiln length as the bed material passes through the kiln. In large kilns with high gas temperatures, the dominant mode of heat transfer to the bed material is by direct gas radiation with some contributions from gas convection, covered inner wall and the exposed inner wall [17]. This holds true in the case of experimental kiln (KDO) where high volumetric natural gas flow

rates were used to attain desired reaction temperatures in the absence of available heat recovery option. High gas velocities resulted in large dust losses ~ 30% of feed material as reported in [3] causing lower percentage filling of bed material. These high excess gas flows results in turbulent conditions for the fluid in the freeboard region. Since radiative heat transfer is proportional to the temperature raised to the fourth power, the thermal resistance between freeboard gas and exposed bed and inner wall decreases with increasing temperature. Such conditions favours close coupling of bed temperature and average value of inside wall temperature at all axial locations. Barr et al [17] has reported minimal differences between the bed and inner wall temperatures in all the trials representing inert bed and an endothermic reactive bed.

With these understandings on kiln feature, the current model was made with multiple sections with each section representing a single temperature joined together in series. Also, the temperature and the radiative properties of combustion gaseous products and the furnace internal wall are assumed constant with the values varying for different sections. At steady state conditions, the energy entering the system delivers a part of the heat to the furnace internal wall by radiation heat transfer and the remainder of the heat passes out in the flue gas. In this model, an engineering approach is made by representing the kiln as a single gas zone surrounded by kiln internal walls with a single value assigned to the composition and temperature of the radiating gas.

The heat transfer  $Q$  between flame (adiabatic temperature) and inner wall is proportional to the difference in gas and wall temperatures raised to the fourth power and effective emissivity and equal to the energy release by combustion gases.

$$Q = (GS)\sigma (T_g^4 - T_w^4) \quad (2)$$

Where  $\sigma$  is the Stefan-Boltzmann constant and  $GS$  is a radiative exchange area available for the gas to inner wall surface (sink), and depends on the gas and sink emissivity and sink geometry.

$$GS = \frac{A_T}{1/\varepsilon_{comb} + 1/C_s \varepsilon_w} - 1 \quad (3)$$

Generally the refractory surface is covered by the raw meal in a typical kiln operation and therefore, the factor  $C_s$ , known as the cold or sink fraction of the internal kiln surface area may possibly be close to unity. For the KDO kiln in operation, the fraction is 0.98 representing the inner wall surface fraction available for heat exchange. The total kiln internal surface area ( $A_T$ ), the wall emissivity ( $\varepsilon_w$ ), and the combined emissivity ( $\varepsilon_{comb}$ ) is represented in Equation 3.

$$\frac{Q}{H_f} = \left( \frac{T_{AFT} - T_g}{T_{AFT} - T_0} \right) \quad (4)$$

To calculate the exit gas temperature ( $T_g$ ) of the medium, the overall energy balance equation includes the feed enthalpy ( $H_f$ ) and the adiabatic flame temperature ( $T_{AFT}$ ) as shown in Equation 4. The adiabatic flame temperature (2,134 K) is estimated by assuming the heat generated during natural combustion is completely transferred to the combustion products without heat loss. Natural gas combustion occurs in 10% excess air at ambient temperature conditions. The standard enthalpy of formation of components ( $\text{CH}_4$ ,  $\text{CO}_2$ ,  $\text{SO}_2$ ,  $\text{H}_2\text{O}$ ,  $\text{O}_2$ ,  $\text{N}_2$ ) as well as their average specific heat capacity over valid temperature range is considered. For reactants and products, the temperature differences between them and the ambient ( $T_0$ ) referred to as base temperature, are large and therefore temperature, as a single value of heat capacity, cannot be considered. A mean specific heat capacity over the temperature range of combustion is thus taken. The coefficients for specific heat capacity as a function of temperature of gases are taken from [20].

The gas temperature is unknown and estimated by equating (2) and (4) where the term  $Q/H_f$  is the ratio of radiation heat flux and gas enthalpy. Figure 6 shows the thermal performance of the pilot scale trial kiln. The temperature measurements were taken on the kiln external surface using the IR camera and validated using the portable thermocouple kit. The external temperature varies from 600 K at the raw feed end to 720 K at the hot flame end. This was done to record indicative temperatures during the production trial and to control the process

operation. Ideally, separate thermocouples for freeboard gas and bed temperatures were needed to be installed inside the kiln for accurate temperature determination. However, with the existing set-up, the bed and freeboard gas temperatures were recorded using bare thermocouples junctions located at regular axial locations. The thermocouple measurements were uncorrected for heat transfer away from it to cool surfaces by radiation. The manufacturer's reported deviation was  $\pm 1.5$  °C for the Type-S (Pt10%Rh-Pt). The actual response of thermocouple was not recorded so to avoid disturbing steady state operation. The thermocouples were rotated with the kiln body, and hence a transient temperature values were obtained between gas and the bed material. Thermocouple measurements reported were 1453 K at the flame side and 800 K towards the feed side. The predicted gas temperatures profiles using the proposed model were 1700 K and 1019 K at the hot flame side and the feed side respectively, were a step different from thermocouple measurements. However, the modelled temperature in the flame zone (1700 K) was validated by the use of thermal imaging IR camera with correction on gas emissivity and associated parameters that reported 1698 K (Figure 3a).

The outer wall heat loss to the surrounding for the entire kiln surface is represented by the total convective and radiative heat losses. The external wall heat loss per unit length was predicted using the measured external wall temperatures. Higher heat losses are predicted at the thermocouple location 1.2 as the burner was inserted up to 1m inside the kiln closer to this location. It appeared from the window that the flame sheet is short (not stratified and long) with possible external recirculation closer to the burner. However, no predictions were made on the type of flame. A highest internal wall temperature of 1087 K is predicted at this same location 1.2 using the external wall temperature data. However, a discrepancy in measured thermocouple gas temperature is observed at the same location which during the trial became unfunctional. The refractory inner wall thickness of 0.05 m with thermal conductivity of 1.6 W/m.K and with the outside natural convective heat transfer coefficient of 20 W/m<sup>2</sup>.K was used. The known kiln internal wall material emissivity of 0.85 is used as discussed

earlier in Section 2.3. Due to the uncertainty in obtaining actual emissivity value, a variability assessment was made by assigning a lower emissivity of 0.7 to the inner wall. Lower emissivity showed only marginal increase in gas temperature profiles with reduction of ~1% in heat transfer efficiency. The maximum external surface heat loss occurred in the flame zone where the external surface is hotter compared to the surface near the raw feed side.

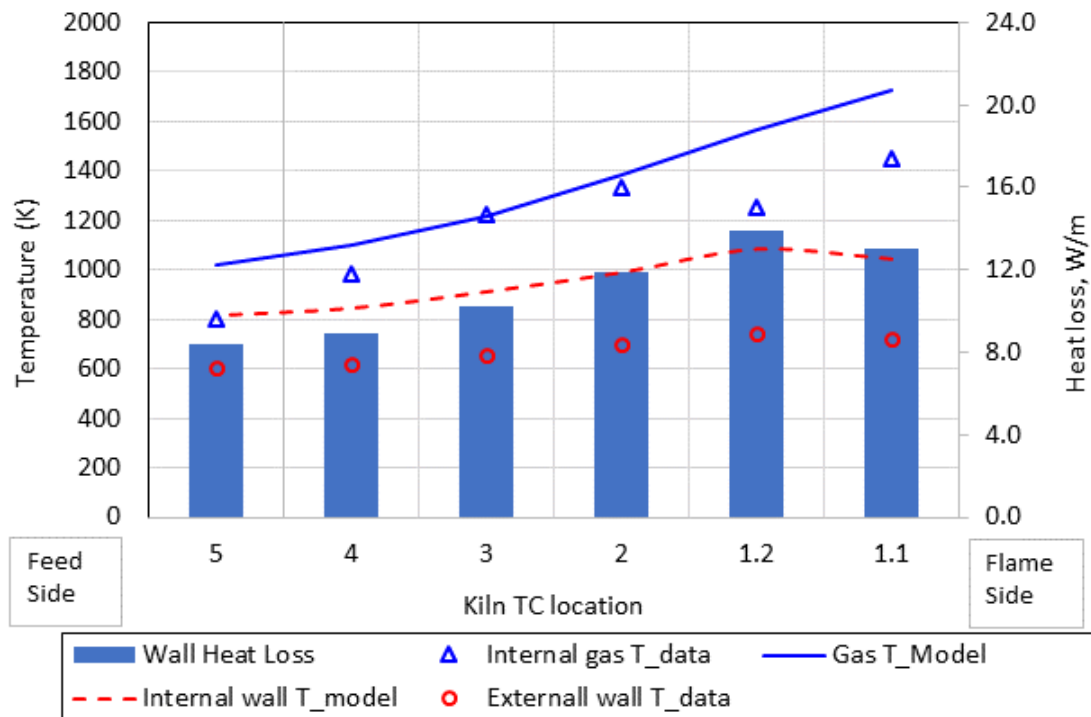


Figure 6. Thermal performance of the pilot scale kiln for CSA clinker.

The total energy balance of the pilot scale KDO kiln is represented by the Sankey diagram in Figure 7. As stated earlier, due to the low thermal efficiency of trial kiln, the temperature in the kiln was maintained in excess of 1500 to 1600 K with average temperature of 1400 K using the excess supply of oxygen along with the natural gas. The total heat input of 214 kW corresponds to the natural gas feed rate of 22 m<sup>3</sup>/hr. Due to high volumetric gas flow rates, significant raw material losses have occurred from the feed side. This resulted in the reduction in anticipated production rates of cement clinker down to approximately 5 kg/hr. The trial kiln was not equipped with any heat recovery option for the flue gas leaving the kiln (132 kW) and resulted in 62% loss with the flue gas. The external wall temperature were

recorded and heat loss was estimated. The combined heat loss due to radiation and convection accounted for 74.8 kW or 35% of total energy input. Therefore, the kiln thermal efficiency was poor with only 3% of the supplied heat transferred to the product clinker.

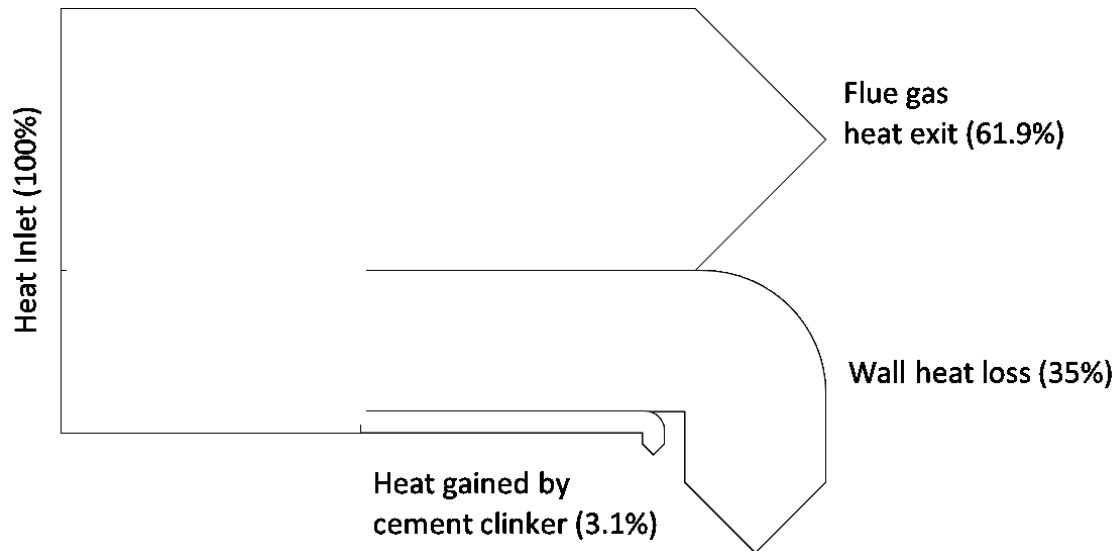


Figure 7. Energy flow within the pilot scale kiln, KDO.

The heat gained is that of the solid input, not of cement clinker. This model can provide approximate performance predictions for the KDO kiln and also for different kiln sizes, pilot-scale or for use in production, and can help to establish the effects of changes in operating parameters on heat transfer trends. It can examine pilot-scale experimental data against predictions and provide insights into the capability of larger, full-scale units.

#### 4. Sensitivity analysis

The evaluation looked at four kilns of varying sizes, as shown in Table 4, for natural gas combustion. A theoretical evaluation to assess the impact of gas radiation on overall kiln heat transfer was carried out. A fixed natural gas feed was used. The gas emissivity increases with kiln size as the optical path length increases. This was reflected in improved kiln heat transfer. The results are summarised in Figure 8. The gas emissivity increases from 0.13 for the KDO kiln to 0.3 for the largest kiln K4. Similarly, the estimated difference in exit gas temperature between the smallest and the largest kiln is 1085 and 952 K respectively. The result show improved heat transfer and increased kiln efficiency with highest efficiency for the largest kiln. The theoretical (adiabatic) flame temperature was used to determine the

overall heat transfer and exit gas temperature. The theoretical maximum thermal efficiency of the smallest kiln was predicted to be ~45% with improvement for larger kilns as shown in terms of efficiency ratio. Industrial size kiln K4 shows 40% improvement over the baseline. However, in reality, K1 was operated in excess natural gas supply to provide enough heat to achieve clinkering temperatures. This kiln has no heat recovery options with an open-to-air viewing window near the flame zone and thin refractory lining. This has contributed to excessive heat losses to the surrounding through the kiln shell and from the flue gas at exit and resulting in very low thermal efficiencies (~3%). By measuring the external shell temperatures an estimate was obtained for the inside wall temperature (950 K) and for the non-adiabatic temperature of the gas inside the kiln. The overall thermal efficiency was predicted to be 23% for inner wall emissivity of 0.85. This is drastically lower than the prediction under adiabatic conditions. This study highlights the capability of the simplistic model to do parametric evaluation in determining the governing parameters.

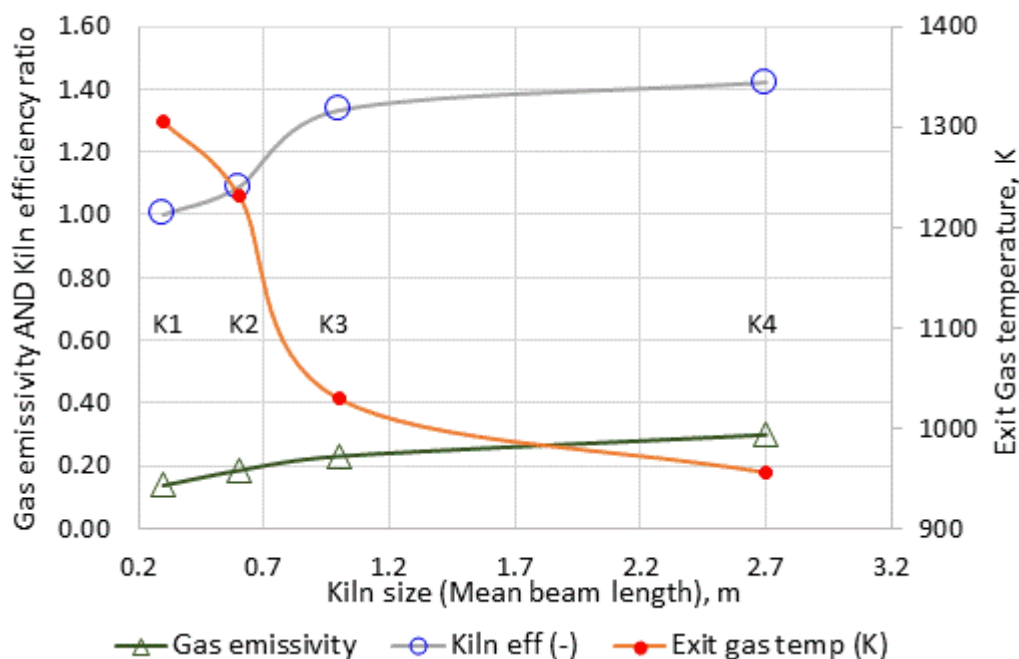


Figure 8. Effect of kiln size on gas emissivity and efficiency.

A more detailed model is necessary to quantify the governing factors of particulate radiation and also the three-way exchange between gas, inner wall lining and the clinker material.

## 5. Discussion

The heat required to facilitate the calcination and clinkering stages within the rotary cement kiln is supplied by burning hydrocarbon fuels. Typically, fuels such as coal or natural gas are fired using the burners to supply the temperatures around 1500 – 1670 K. The partial pressures (or concentrations) of combustion gases (mainly CO<sub>2</sub> and H<sub>2</sub>O) are determined by the combustion environment such as the type of fuel used and excess air/O<sub>2</sub>. The levels of concentration of these gases are expected to have an impact on the furnace radiative heat transfer. In addition, contribution of radiation emitted by the particulate matter is important towards increasing the luminosity of flames. For coal combustion, the radiative properties of particulates (char, soot, ash) will depend on particle size, shape, volume fraction, chemical composition and temperature. The contribution of particulate emissivity will increase with furnace size and becomes important towards determining overall kiln heat transfer. In case of gaseous radiation, the high heat capacity of CO<sub>2</sub> and H<sub>2</sub>O and higher gas emissivity will influence the radiation heat transfer. Typically, the ratio of partial pressures (P<sub>H<sub>2</sub>O</sub>/P<sub>CO<sub>2</sub></sub>) in the case of coal-fired kilns is 0.5, compared to 1.8 for natural gas fired burners. The model presented for gas radiation estimation [13] utilises the 3-GGM model, which is widely used in many CFD commercial codes. The model is limited in use for optical path lengths of upto 10 atm-m and applicable for partial pressure ratios of water vapour to carbon dioxide of 1 to 2. Therefore, an appropriate gas radiation model needs to be selected depending on the fuel used (coal/natural gas) and the size of kiln to develop an overall kiln heat transfer model.

## 6. Conclusions

The technical feasibility of the production of novel CSA cement clinker with elemental sulfur combustion (as a replacement of sulfur source from traditional calcium sulfate feed) was successfully achieved using the pilot scale kiln. The pilot scale demonstration highlights the feasibility of using sulfur by-product sourced from the sour gas stripping operation, can provide partial or complete replacement of calcium sulfate.

A simple heat transfer model was developed to predict the overall heat transfer performance of the KDO kiln. The thermal performance was validated by the experimental measurements of internal gas and external surface temperatures. The predicted gas temperatures vary from 1724 K at the hot end to 1019 K at the kiln exit. The pilot kiln had no heat recovery mechanism and majority (61.9%) of heat associated with flue gas was lost at the exit, 35% through the outer wall heat losses and therefore, had a very low thermal efficiency of 3%.

Scale-up studies show the gas radiation differences exist, depending on kiln size and fuel type used. This has an impact on kiln thermal performance. This work has demonstrated that a simple heat transfer model can be effectively used to predict scale-up effects. However, detailed modelling is required for more accurate predictions. Large-scale production trials for the novel cement clinkers are proposed.

An important conclusion of this research is it provides a scientific basis for our understanding of scale effects that underpins our use of pilot-scale rotary kiln trials. The simplistic model can be extended and refined in future with more detailed and computationally intense CFD based models.

## Acknowledgements

The authors gratefully acknowledge the financial support of Gulf Organisation for Research and Development (GORD), University of Aberdeen grant number EG016-RG11757. They also offer sincere thanks to Dr Thomas Matschei and Mr Guanshu Li at LafargeHolcim for the stimulating discussions relating to future commercial development of CSA. Finally, the authors wish to thank the engineering and operational support team at IBU-tec, who helped to manage and carry out the pilot-scale trials.

## References

- [1] E. Gartner, Industrially interesting approaches to 'low-CO<sub>2</sub>' cements, *Cement and Concrete Research*, 34(9) (2004) 1489-1498.
- [2] I. Galan, F.P. Glasser, A. Elhoweris, S. Tulley, A Murdoch, Novel process for calcium sulfo-aluminate cement production, 34<sup>th</sup> Cement and Concrete Conference (2014) 203.
- [3] T. Hanein, I. Galan, A. Elhoweris, S. Khare, S. Skalamprinos, G. Jen, M. Whittaker, M. S. Imbabi, F. P. Glasser, M. N. Bannerman, Production of belite calcium sulfoaluminate

- cement using sulfur as a fuel and as a source of clinker sulfur trioxide-Pilot kiln trial, *Advances in Cement Research*, 28(10) (2016) 643-653.
- [4] E. Mastorakos, A. Massias et al., CFD predictions for cement kilns including flame modelling, heat transfer and clinker chemistry, *Applied Mathematical Modelling*, 23(1999) 55-76.
- [5] Koukkari, P., *Advanced Gibbs Energy Methods for Functional Materials and Processes. Research Notes*, (2009) 2506.
- [6] Meyer, V., et al., Computation of steady state thermochemistry in rotary kilns: Application to the cement clinker manufacturing process. *Chemical Engineering Research and Design*, 115 (2016) 335-347.
- [7] Romero Valle, M.A., *Numerical Modelling of Granular Beds in Rotary Kilns*. 2012, Delft University of Technology.
- [8] Li, S.Q., et al., A Mathematical Model of Heat Transfer in a Rotary Kiln Thermo-Reactor. *Chemical engineering & technology*, 28(12) (2005) 1480-1489.
- [9] Mujumdar, K.S. and V.V. Ranade, Simulation of rotary cement kilns using a one-dimensional model. *Chemical Engineering Research and Design*, 84(3) (2006) 65-177.
- [10] <http://www.roessel-messtechnik.de/rm-ru/>
- [11] T.Hanein, F.P.Glasser, M. Bannerman, Thermodynamics of Portland cement clinkering, 14<sup>th</sup> International Congress on the chemistry of cement (ICCC) Beijing, China, (2015).
- [12] <http://www.flir.co.uk>
- [13] T.F.Smith, Z.F.Shen, J.N.Friedman, Evaluation of coefficients for the weighted sum of gray gases model, *Transactions of the ASME*, 104 (4) (1982) 602-608.
- [14] G.A. Ketslakh, I.P. Tsibin, Heat transfer by radiation in rotary kilns, *Eastern institute of refractories*, No.1 (1978) 17-19.
- [15] K.S. Mujumdar, V.V. Ranade, Modelling of rotary cement kilns: Applications to reduction in energy consumption, *Ind. Eng. Chem.Res.* 45 (2006) 2315-2330.
- [16] H.C. Hottel, A.F. Sarofim, *Radiative transfer*, vol.1, New York: McGraw-Hill, Inc. pp 459, 1967.
- [17] P.V. Barr, J.K. Brimacombe, A.P. Watkinson, A heat transfer model for the rotary kiln-I, Pilot kiln trials, *Metallurgical Transactions B*, (20B) (1989) 391-402.
- [18] K.S. Mujumdar, V.V. Ranade, CFD modelling of rotary cement kilns, *Asia-Pacific Journal of Chemical Engineering*, 3 (2008) 106-118.
- [19] J.P. Gorog, J.K. Brimacombe, T.N. Adams, Radiative heat transfer in rotary kilns, *Metallurgical Transactions B*, (12) (1981) 55-70.
- [20] R.C. Reid, T.K. Sherwood, *The properties of gases and liquids*, McGraw-Hill, 3<sup>rd</sup> Edition, 1977.